J Mater Sci: Mater Electron (2016) 27:4321–4325
DOI 10.1007/s10854-016-4299-6

Synthesis, characterization and optical properties of lutetium doped nickel ferrite nanoparticles prepared by novel sol–gel method

Ruhollah Talebi[1] · **Amin Alborzi**[1]

Received: 9 October 2015 / Accepted: 6 January 2016 / Published online: 30 January 2016

Abstract Lutetium doped nickel ferrite nanoparticles were successfully synthesized by novel sol–gel method with the aid of nickel(II) nitrate, iron(III) nitrate, lutetium(III) nitrate and lactose without adding external surfactant. Moreover, lactose plays role as capping agent, reducing agent, and natural template in the synthesis $NiFe_{2-x}Lu_xO_4$ nanoparticles. The as-synthesized $NiFe_{2-x}Lu_xO_4$ nanoparticles were characterized by means of several techniques such as X-ray diffraction, scanning electron microscopy, energy dispersive X-ray microanalysis and UV–Vis diffuse reflectance spectroscopy. The magnetic properties of as-prepared $NiFe_{2-x}Lu_xO_4$ nanoparticles were also investigated with vibrating sample magnetometer. To evaluate the photocatalyst properties of nanocrystalline $NiFe_{2-x}Lu_xO_4$, the photocatalytic degradation of methyl orange under ultraviolet light irradiation was carried out.

1 Introduction

Physical properties and potential applications of nanostructures and nanomaterial have been studied intensively [1–3]. This interest results from the special properties of materials at the nanoscale, such as a large surface-to-volume ratio and increased surface activity, as compared with that of the bulk material. The properties of bulk materials usually depend on the size of the primary particles. Thus, the control of particle size and morphology plays a crucial role in the manufacturing process [4–8]. In ferrite MFe_2O_4, the choice of rare-earth ions allows a relative tenability of the magnetic properties such as magnetization or anisotropy. The presence of rare-earth ions influences mainly the magnetic anisotropy of the system. The octahedral and tetrahedral sublattice magnetizations are antiparallel and therefore a noncompensated magnetic moment occurs. This structure is called ferrimagnetic. Various properties such as superparamagnetism [9, 10] and spin canting [11, 12] are observed when the particle size is much reduced compared to the bulk materials. Spinel-type ferrites powders can be prepared by ceramic technique [13], evaporative decomposition of metal organic solution [14], co-precipitation [15], sol–gel [16–18], microemution [19], micelle and hydrothermal methods [20, 21]. However, some methods encounter problems such as the formation of the undesirable phase, the requirement of complicated equipment or time-consuming caused by multiple steps, etc. Photocatalysis is a subject of current interest related to its application in effluent decontamination. Photocatalytic degradation of organic pollutants is becoming one of the most promising green chemistry technologies. In most of the industries, phenolic compounds are widely used and have become common pollutants in waste water bodies. The phenolic compounds are quite stable and remain in the environment for a long period of time. Due to their toxicity and carcinogenic character, they are dangerous to the ecosystem in water bodies and human health. A representative of this class of compounds is phenol. Sources of phenol include the process or waste solutions in chemical process industries, agriculture production, etc. [4, 6, 7]. In the present study, an attempt has been made to synthesis Lu^{3+} doped $NiFe_2O_4$ nanoparticles by the novel sol gel method. The photocatalytic degradation was investigated using methyl orange (MO) under ultraviolet light irradiation.

✉ Amin Alborzi
alborziamin74@gmail.com

[1] Young Researchers and Elite Club, Central Tehran Branch, Islamic Azad University, Tehran, Iran

2 Experimental

2.1 Characterization

X-ray diffraction (XRD) patterns were recorded by a Philips-X'PertPro, X-ray diffractometer using Ni-filtered Cu K_α radiation at scan range of $10 < 2\theta < 80$. Scanning electron microscopy (SEM) images were obtained on LEO-1455VP equipped with an energy dispersive X-ray spectroscopy. The energy dispersive spectrometry (EDS) analysis was studied by XL30, Philips microscope. The magnetic measurement of samples were carried out in a vibrating sample magnetometer (VSM) (Meghnatis Daghigh Kavir Co.; Kashan Kavir; Iran) at room temperature in an applied magnetic field sweeping between ±10,000 Oe. Spectroscopy analysis (UV–Vis) was carried out using shimadzu UV–Vis scanning UV–Vis diffuse reflectance spectrometer.

2.2 Synthesis of $NiFe_{2-x}Lu_xO_4$ nanoparticles

Nickel(II) nitrate, iron(III) nitrate, and lutetium(III) nitrate with a stoichiometric ratio of 1:1.95:0.05, were dissolved separately in 30 ml of water under magnetic stirring to form a homogeneous solution. Then, a solution containing 1 mmol of lactose was added into a solution involving 1 mmol of $Ni(NO_3)_2{\cdot}6H_2O$. Subsequently, above mention solution was mixed with solution containing 1.95 mmol of $Fe(NO_3)_3{\cdot}9H_2O$, and 0.05 mmol $Lu(NO_3)_3{\cdot}6H_2O$. Afterwards, the final mixed solution was kept stirring to form a gel at 110 °C. Finally, the obtained product was placed in a conventional furnace in air atmosphere for 2 h and calcine at 800 °C. After thermal treatment, the system was allowed to cool to room temperature naturally, and the obtained precipitate was collected.

2.3 Photocatalysis experiments

The methyl orange (MO) photodegradation was examined as a model reaction to evaluate the photocatalytic activities of the $NiFe_{2-x}Lu_xO_4$ nanoparticles. The photocatalytic experiments were performed under an irradiation ultraviolet light. The photocatalytic activity of nanocrystalline $NiFe_{2-x}Lu_xO_4$ obtained was studied by the degradation of methyl orange solution as a target pollutant. The photocatalytic degradation was performed with 50 ml solution of methyl orange (0.0005 g) containing 0.1 g of $NiFe_{2-x}Lu_xO_4$. This mixture was aerated for 30 min to reach adsorption equilibrium. Later, the mixture was placed inside the photoreactor in which the vessel was 15 cm away from the ultraviolet source of 400 W mercury lamps. The photocatalytic test was performed at room temperature. Aliquots of the mixture were taken at definite interval of times during the irradiation, and after centrifugation they were analyzed by a UV–Vis spectrometer. The methyl orange (MO) degradation percentage was calculated as:

$$\text{Degradation rate}\,(\%) = 100\,(A_0 - A_t)/A_0 \quad (1)$$

where A_t and A_0 are the obtained absorbance value of the methyl orange solution at t and 0 min by a UV–Vis spectrometer, respectively.

3 Results and discussion

Crystalline structure and phase purity of as-prepared product has been determined using XRD. The XRD pattern of the $NiFe_2O_4$ in presence of La^{3+} doped is shown in Fig. 1. The XRD pattern of the as-synthesized $NiFe_{2-x}Lu_xO_4$ nanoparticles (Fig. 1) indicates the formation of cubic phase of $NiFe_{2-x}Lu_xO_4$ (JCPDS No. 03-0875) with the calculated cell parameter of $a = b = c = 8.3400$ Å. According to XRD data, the crystallite diameter (D_c) of $NiFe_{2-x}Lu_xO_4$ nanoparticles are calculated to be 48 nm using the Scherer Eq. (1):

$$D_c = K\lambda/\beta\cos\theta \quad (2)$$

where β is the breadth of the observed diffraction line at its half intensity maximum, K is the so-called shape factor, which usually takes a value of about 0.9, and λ is the wavelength of X-ray source used in XRD. The morphology of the nanoparticles was investigated using SEM which demonstrates uniform nanoparticles with spherical shape homogenously distributed all over the sample, as it could be clearly observed in Fig. 2. The $NiFe_{2-x}Lu_xO_4$ nanoparticles with particle size of about 55–60 nm were observed. The EDS analysis measurement was used to investigate the chemical composition and purity of $NiFe_{2-x}Lu_xO_4$ nanoparticles. According to the Fig. 3, the product consists of Ni, Fe, Lu, and O elements. Furthermore, neither N nor C signals were detected in the EDS spectrum, which means the product is pure and free of any surfactant or impurity. The hysteresis loop of $NiFe_{2-x}Lu_xO_4$ nanoparticles was studied to examine their magnetic properties (Fig. 4). At 300 K the remanent magnetization (M_r) is 4 emu/g, the coercive field (H_c) is 90 Oe and the magnetization at saturation (M_s) is estimated to be only 23 emu/g (the saturation magnetization M_s was determined from the extrapolation of curve of H/M vs. H). The diffused reflectance spectrum of the as-prepared $NiFe_{2-x}Lu_xO_4$ nanoparticles is shown in Fig. 5. The fundamental absorption edge in most semiconductors follows the exponential law. Using the absorption data the band gap was estimated by Tauc's relationship:

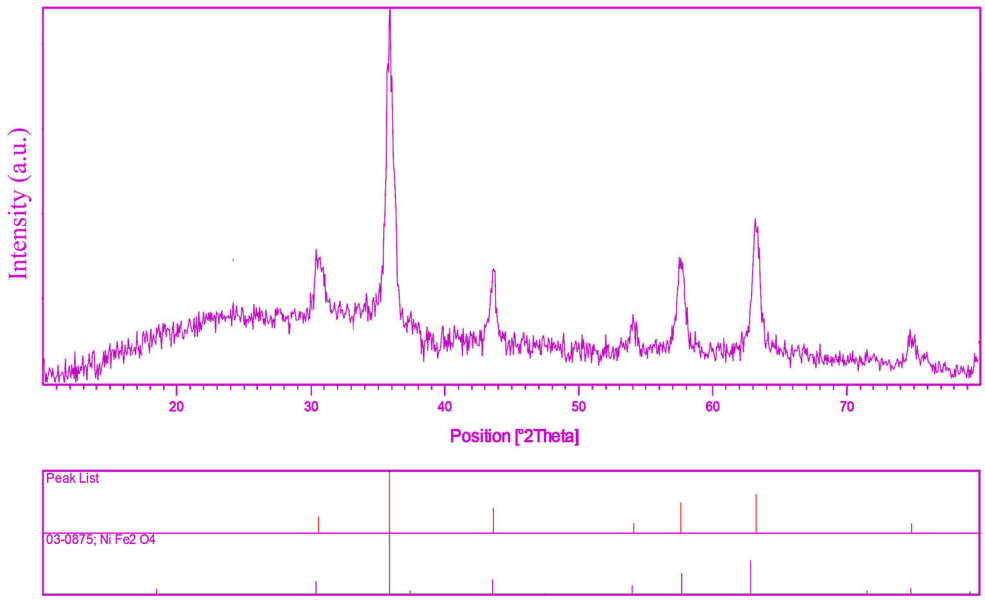

Fig. 1 XRD pattern of $NiFe_{2-x}Lu_xO_4$ nanoparticles calcined at 800 °C

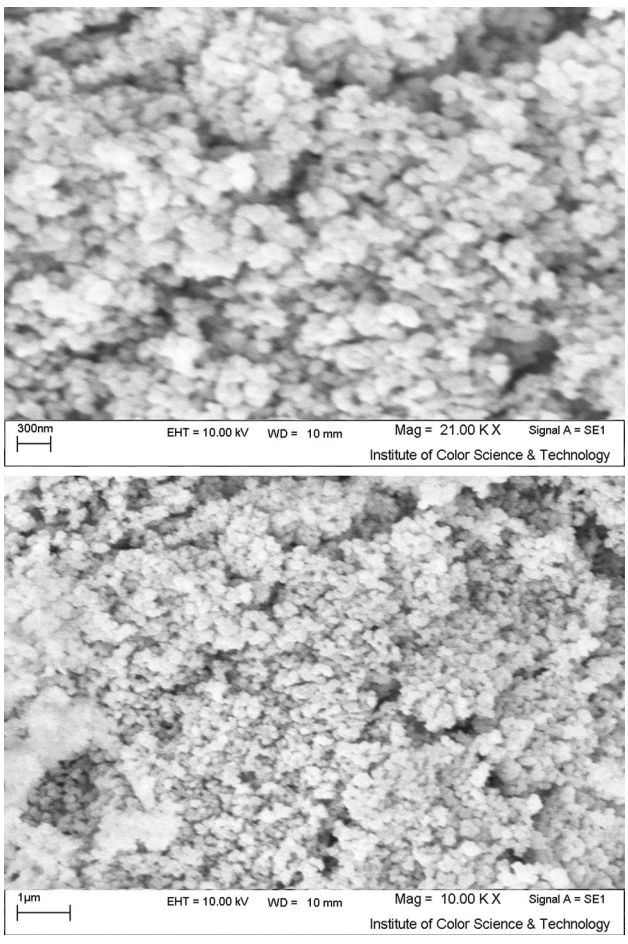

Fig. 2 SEM image of $NiFe_{2-x}Lu_xO_4$ nanoparticles calcined at 800 °C

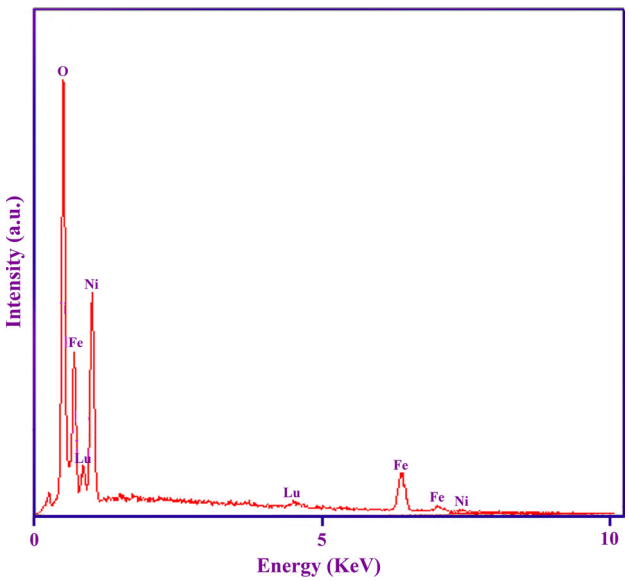

Fig. 3 EDS pattern of $NiFe_{2-x}Lu_xO_4$ nanoparticles calcined at 800 °C

$$\alpha = \alpha 0\left(h\nu - E_g\right)n/h\nu$$

where α is absorption coefficient, hν is the photon energy, α0 and h are the constants, E_g is the optical band gap of the material, and n depends on the type of electronic transition and can be any value between ½ and 3. The energy gap of the $NiFe_{2-x}Lu_xO_4$ nanoparticles is determined by extrapolating the linear portion of the plots of $(\alpha h\nu)^2$ against hν to the energy axis, as shown in Fig. 5. The E_g value is

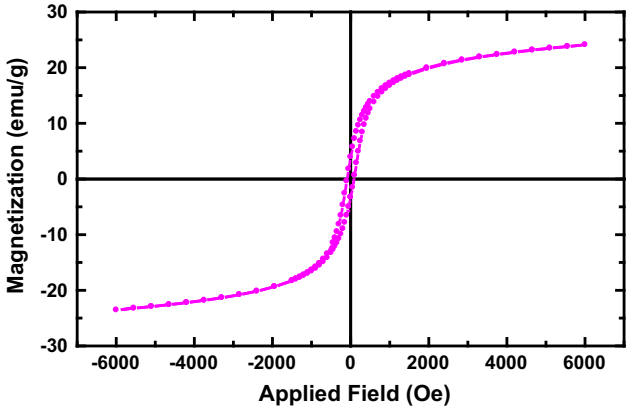

Fig. 4 VSM curves of $NiFe_{2-x}Lu_xO_4$ nanoparticles calcined at 800 °C

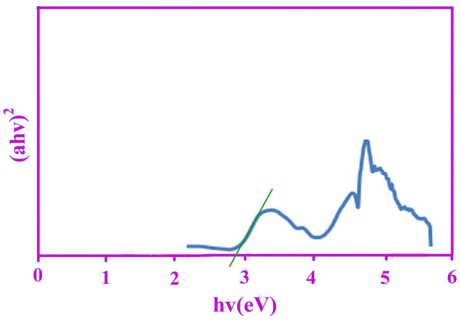

Fig. 5 UV–Vis pattern of $NiFe_{2-x}Lu_xO_4$ nanoparticles calcined at 800 °C

calculated as 2.8 eV for the $NiFe_{2-x}Lu_xO_4$ nanoparticles. Photodegradation of methyl orange under UV light irradiation (Fig. 6a–c) was employed to evaluate the photocatalytic activity of the as-synthesized $NiFe_{2-x}Lu_xO_4$. No methyl orange was practically broken down after 60 min without using UV light irradiation or nanocrystalline $NiFe_{2-x}Lu_xO_4$. This observation indicated that the contribution of self-degradation was insignificant. The mechanism for the enhanced photocatalysis of $NiFe_{2-x}Lu_xO_4$ could be proposed as follow. Under the irradiation, the electrons (e^-_{cb}) are excited from the valence band to the conduction band of $NiFe_{2-x}Lu_xO_4$ leaving behind h^+_{vb}. Lu doping in $NiFe_{2-x}Lu_xO_4$ being lewis acid due to the presence of partially filled orbital can effectively trap the e^-_{cb} and inhibit the recombination with h^+_{vb}. This suggested that the Lu dopant can serve as an effective charge carrier trap and facilitated the excited e^-_{cb} transfer under visible light irradiation. The degradation mechanism for the $NiFe_{2-x}Lu_xO_4$ can be given as:

$$NiFe_{2-x}Lu_xO_4 + h\nu \rightarrow NiFe_{2-x}Lu_xO_4^{\cdot} + e^- + h^+ \quad (3)$$

$$h^+ + H_2O \rightarrow OH^{\cdot} \quad (4)$$

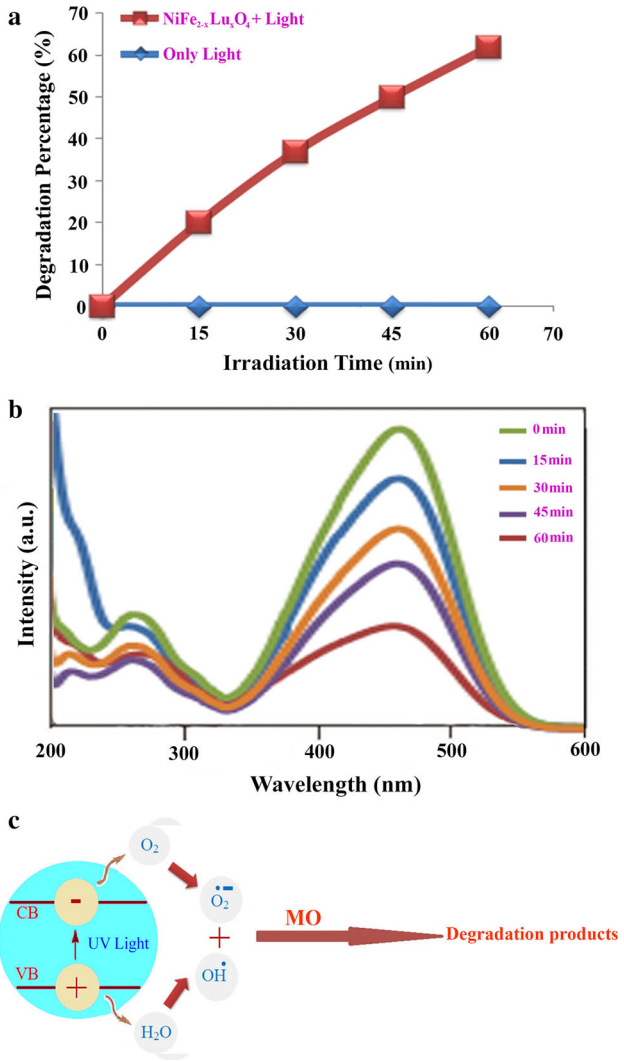

Fig. 6 Photocatalytic methyl orange degradation of $NiFe_{2-x}Lu_xO_4$ nanoparticles under ultraviolet light (**a**), fluorescence spectral time scan of methyl orange illuminated at 510 nm with $NiFe_{2-x}Lu_xO_4$ nanoparticles (**b**), and reaction mechanism of methyl orange photodegradation over $NiFe_{2-x}Lu_xO_4$ under ultraviolet light irradiation (**c**)

$$e^- + O_2 \rightarrow O_2^{\cdot -} \quad (5)$$

$$OH^{\cdot} + O_2^{\cdot -} + \text{methyl orange} \rightarrow \text{Degradation products} \quad (6)$$

Using photocatalytic calculations by Eq. (1), the methyl orange degradation was about 63 % after 60 min irradiation of UV light, and nanocrystalline $NiFe_{2-x}Lu_xO_4$ presented high photocatalytic activity (Fig. 6a). The spectrofluorimetric time-scans of methyl orange solution illuminated at 510 nm with nanocrystalline $NiFe_{2-x}Lu_xO_4$ are depicted in Fig. 6b. Figure 6b shows continuous removal of methyl

orange on the $NiFe_{2-x}Lu_xO_4$ under UV light irradiation. It is generally accepted that the heterogeneous photocatalytic processes comprise various steps (diffusion, adsorption, reaction, and etc.), and suitable distribution of the pore in the catalyst surface is effective and useful to diffusion of reactants and products, which prefer the photocatalytic reaction. In this investigation, the enhanced photocatalytic activity can be related to appropriate distribution of the pore in the nanocrystalline $NiFe_{2-x}Lu_xO_4$ surface, high hydroxyl amount and high separation rate of charge carriers (Fig. 6c). Furthermore, this route is facile to operate and very suitable for industrial production of $NiFe_{2-x}Lu_xO_4$ nanoparticles.

4 Conclusions

In this work, $NiFe_{2-x}Lu_xO_4$ nanoparticles were successfully synthesized by a novel sol-gel method at 800 °C for 120 min. The stages of the formation of $NiFe_{2-x}Lu_xO$, as well as the characterization of the resulting compounds were done using X-ray diffraction and energy dispersive X-ray spectroscopy. The products were analyzed by scanning electron microscopy (SEM), and ultraviolet–visible (UV–Vis) spectroscopy to be round, about 55–60 nm in size and $E_g = 2.8$ eV. The magnetic properties of the as-synthesized products were also studied. When as-prepared nanocrystalline $NiFe_{2-x}Lu_xO$ was utilized as photocatalyst, the percentage of methyl orange degradation was about 63 % after 60 min irradiation of UV light.

Acknowledgments Authors are grateful to council of University of Central Tehran for providing financial support to undertake this work.

Compliance with ethical standards

Conflict of interest The author declares that the research was conducted in the absence of any commercial or financial relationships that could be construed as a potential conflict of interest.

References

1. Y. Zhang, Y. Zhang, B. Fu, M. Hong, M. Xiang, Z. Liu, J. Leng, J. Mater. Sci. Mater. Electron. **25**, 5475 (2014)
2. Z. Khayat Sarkar, F. Khayat Sarkar, Int. J. Nanosci. Nanotechnol. **7**, 197 (2011)
3. A. Ghasemi, A.M. Davarpanah, M. Ghadiri, Int. J. Nanosci. Nanotechnol. **8**, 207 (2012)
4. F.S. Ghoreishi, V. Ahmadi, M. Samadpourc, J. Nanostruct. **3**, 453 (2013)
5. S. Moshtaghi, D. Ghanbari, M. Salavati-Niasari, J. Nanostruct. **5**, 169 (2015)
6. A. Rahdar, M. Aliahmad, Y. Azizi, J. Nanostruct. **5**, 145 (2015)
7. J. Safaei-Ghomi, S. Zahedi, M. Javid, M.A. Ghasemzadeh, J. Nanostruct. **5**, 153 (2015)
8. D. Li, R. Shi, C. Pan, Y. Zhu, H. Zhao, Cryst. Eng. Comm. **13**, 4695 (2011)
9. C.P. Bean, J.D. Livingston, J. Appl. Phys. **30**, 120 (1959)
10. D.L. Leslie-Pelecky, R.D. Rieke, Chem. Mater. **8**, 1770 (1996)
11. A.T. Ngo, P. Bonville, M.P. Pileni, J. Appl. Phys. **89**, 3370 (2001)
12. S.A. Oliver, H.H. Hamdeh, J.C. Ho, Phys. Rev. B **99**, 3400 (1829)
13. A. Lakshman, P.S.V. Subba Rao, K.H. Rao, J. Magn. Magn. Mater. **284**, 352 (2004)
14. Q. Song, Z.J. Zhang, J. Am. Chem. Soc. **126**, 6164 (2004)
15. S. Dey, A. Roy, J. Ghose, J. Appl. Phys. **90**, 4138 (2001)
16. Z. Yue, J. Zhou, X. Wang, Z. Gui, L. Li, J. Eur. Ceram. Soc. **23**, 189 (2003)
17. X.M. Liu, S.Y. Fu, C.J. huang. J. Magn. Magn. Mater. **281**, 234 (2004)
18. K.P. Chae, J.G. Lee, H.S. Kweon, Y.B. Lee, J. Magn. Magn. Mater. **283**, 103 (2004)
19. M. Bonini, A. Wiedenmann, P. Baglioni, Phys. A **339**, 86 (2004)
20. X. Li, C. Kutal, J. Alloys Comput. **349**, 264 (2003)
21. H.W. Wang, S.C. Kung, J. Magn. Magn. Mater. **270**, 230 (2004)